



Deposited via The University of Sheffield.

White Rose Research Online URL for this paper:

<https://eprints.whiterose.ac.uk/id/eprint/147005/>

Version: Accepted Version

---

**Article:**

Alsaif, A., Garcia, R., Figueiredo, F.P. et al. (2019) Fatigue performance of flexible steel fibre reinforced rubberised concrete pavements. *Engineering Structures*, 193. pp. 170-183. ISSN: 0141-0296

<https://doi.org/10.1016/j.engstruct.2019.05.040>

---

Article available under the terms of the CC-BY-NC-ND licence  
(<https://creativecommons.org/licenses/by-nc-nd/4.0/>).

**Reuse**

This article is distributed under the terms of the Creative Commons Attribution-NonCommercial-NoDerivs (CC BY-NC-ND) licence. This licence only allows you to download this work and share it with others as long as you credit the authors, but you can't change the article in any way or use it commercially. More information and the full terms of the licence here: <https://creativecommons.org/licenses/>

**Takedown**

If you consider content in White Rose Research Online to be in breach of UK law, please notify us by emailing [eprints@whiterose.ac.uk](mailto:eprints@whiterose.ac.uk) including the URL of the record and the reason for the withdrawal request.

# Fatigue Performance of Flexible Steel Fibre Reinforced Rubberised Concrete Pavements

Abdulaziz Alsaif<sup>a,b\*</sup>, Reyes Garcia<sup>a,c</sup>, Fabio P. Figueiredo<sup>a</sup>, Kyriacos Neocleous<sup>d</sup>,  
Andreas Christofe<sup>d</sup>, Maurizio Guadagnini<sup>a</sup>, Kypros Pilakoutas<sup>a</sup>

<sup>a</sup>Department of Civil and Structural Engineering, The University of Sheffield, Sir Frederick Mappin Building, Mappin Street, Sheffield, S1 3JD, UK.

<sup>b</sup>Department of Civil Engineering, King Saud University, P. O. Box 800, Riyadh 11421, Saudi Arabia.

<sup>c</sup>School of Engineering, The University of Warwick, Library Road, Coventry, CV4 7AL, UK.

<sup>d</sup>Department of Civil Engineering and Geomatics, Cyprus University of Technology, Achilleos 1 Building, Saripolou 2-8, P.O.Box 50329, 3603 Limassol, CY, Cyprus.

Corresponding author: email: [asaalsaif1@sheffield.ac.uk](mailto:asaalsaif1@sheffield.ac.uk); Tel: +44 (0) 114 222 5729,

*Fax: +44 (0) 114 2225700*

## Abstract

Recycled rubber particles and steel fibres from end-of-life tyres have the potential to enhance the flexibility and ductility of concrete pavements and produce more sustainable pavement solutions. However, the fatigue behaviour of such pavements is not fully understood. This article investigates the mechanical and fatigue performance of steel fibre reinforced concrete (SFRC) and steel fibre reinforced rubberised concrete (SFRRuC). Specimens tested were cast using rubber particles as replacement of natural aggregates (0%, 30% and 60% by volume), and using a blend of manufactured and recycled tyre steel fibres (40 kg/m<sup>3</sup>). Prisms were subjected to four-point flexural cyclic load ( $f=15$  Hz) at stress ratios of 0.5, 0.7, 0.8 and 0.9. The results show that, compared to plain concrete, the addition of steel fibres alone improves the fatigue stress resistance of concrete by 11% (at 25% probability of failure). The replacement of natural aggregates with rubber particles improves the flexibility of SFRRuC (from 51 GPa elastic modules for plain concrete to 13 GPa for SFRRuC), but reduces its fatigue stress resistance by 42% (at 25% probability of failure). However, a probabilistic analysis of the fatigue life data and overall design considerations show that the flexible SFRRuC can be used for pavements. To account for the effect of fatigue load, the Concrete Society approach included in TR34 is modified to account for SFRRuC pavements. Finite element analyses show that flexible SFRRuC pavements can accommodate large subgrade movements and settlements and result in much smaller cracks (up to 24 times) compared to SFRC pavements.

37 **Keywords:** *Rubberised concrete; Fatigue performance; Steel fibre reinforced rubberised*  
38 *concrete; Flexible concrete pavement; Recycled fibres*

## 39 **1 Introduction**

40

41 Rigid concrete pavements are widely used in the construction of long-lasting roads as they  
42 enable a better distribution of load over the subgrade and require overall smaller structural  
43 depth, compared to flexible asphalt pavements. However, road pavement slabs are subjected to  
44 continuous cyclic traffic and thermal loads that can deteriorate the material mechanical  
45 properties, propagate cracks and eventually cause fatigue fracture [1-3], leading to premature  
46 pavement failure. A potential solution to enhance the flexibility, toughness and fatigue  
47 resistance of concrete pavements is to replace part of the natural aggregates with waste tyre  
48 rubber (WTR) particles [4, 5]. Rubber aggregates are known to reduce stiffness and enhance  
49 impact and skid resistance of concrete [6-12], but can cause significant decrease in mechanical  
50 properties, especially at high rubber contents (up to 90% reduction in compressive strength for  
51 100% natural aggregates replacement) [13-17]. Consequently, until now rubberised concrete  
52 (RuC) is mainly utilised in low-strength non-structural applications, e.g. concrete pedestrian  
53 blocks [11]. Few researchers studied the performance of RuC in structural applications and to  
54 date there are limited studies on the fatigue performance of RuC [7, 18-23]. Liu et al. [7] studied  
55 the effect of replacing small percentages of fine natural aggregates with crumb rubber particles  
56 (0 to 15% by volume) and found that the fatigue performance of the RuC mixes was better than  
57 that of ordinary concrete. The enhancement was attributed to the ability of rubber to resist crack  
58 propagation by filling internal spaces and absorbing energy through deformation.

59

60 To enhance the strength of RuC for structural applications (especially flexural strength), steel  
61 fibres can be used to produce steel fibre reinforced rubberised concrete (SFRRuC) [5, 20, 24-  
62 26]. In SFRRuC, rubber particles absorb energy and enhance the fracture characteristics of the  
63 material [14, 27], whereas the fibres control crack opening and propagation even after the peak  
64 load, thus dissipating energy through gradual fibre debonding [8]. Ganesan et al. [20] examined  
65 the flexural fatigue behaviour of self-compacting RuC (SCRuC) with and without  
66 manufactured steel fibres. They observed that the replacement of fine aggregates with crumb  
67 rubber particles (up to 20% by volume) improved the flexural fatigue strength by  
68 approximately 15%. The addition of crimped-type manufactured steel fibres (MSF) into  
69 SCRuC mixes further enhanced the fatigue strength by 10%. More recently, Gupta et al. [22]  
70 reported that the incorporation of rubber ash and rubber fibres in concrete as a replacement of  
71 fine natural aggregates (up to 35% by volume) enhanced the flexural impact and fatigue  
72 resistance by up to 217% and 52%, respectively.

73 Whilst these studies examined the fatigue of mixes with small amounts of rubber (less than  
74 20% by total aggregate volume), recent research [8] has proven that the use of large amounts  
75 of rubber (especially large rubber particles) is necessary to attain low stiffness pavements with  
76 the potential to accommodate subgrade movements. The authors [8] have recently proposed  
77 optimised flexible SFRRuC mixes with large amounts of rubber (60% by volume replacement  
78 of natural aggregates) and blends of MSF and recycled tyre steel fibres (RTSF) that meet the  
79 flexural strengths of EN 13877-1 [28]. The authors [29, 30] also demonstrated that the  
80 durability, long-term and permeability performance indicators of the optimised mixes, rank  
81 them as ‘highly durable concrete’[31-34]. These properties make SFRRuC a promising  
82 candidate for sustainable road pavement slabs, particularly considering that reusing end-of-life  
83 tyre materials (WTR and RTSF) in concrete would contribute to the reduction of the  
84 environmental impact caused by discarded tyres (1.5 billion units/year [35]). However, to date,  
85 the flexural fatigue performance of SFRRuC with large amounts of rubber and steel fibres has  
86 not been investigated.

87  
88 As the variability in flexural fatigue performance of steel fibre reinforced concrete (SFRC) and  
89 SFRRuC is expected to be high due to the combination of rubber and/or fibres [20, 22], a  
90 statistical approach may need to be adopted to quantify the reliability of experimental results  
91 and their suitability for use in pavement design. Probabilistic distribution models including the  
92 two-parameter Weibull distribution model, graphical interpolation model and the mathematical  
93 model are commonly used to statistically analyse fatigue life data and derive probabilistic  
94 relationships that can be used in design [1, 36, 37].

95  
96 This study assesses the mechanical and fatigue performance of SFRRuC. Initially, the study  
97 examines the mechanical performance of SFRC and SFRRuC mixes with different replacement  
98 volumes of rubber aggregates (0, 30 and 60%) and a blend of MSF and RTSF. The results are  
99 compared in terms of uniaxial compressive strength, static flexural strength, elastic modulus,  
100 and flexural fatigue strength (number of fatigue cycles). Subsequently, three different  
101 probabilistic approaches are used to estimate the fatigue life. The design implications of using  
102 SFRRuC in new pavements is shown by a practical example. Finite element analyses are  
103 performed using Abaqus® to demonstrate the capability of flexible SFRRuC pavements to  
104 accommodate subgrade movements and settlements. This study contributes towards  
105 developing economically and structurally sound alternative materials for sustainable flexible  
106 concrete pavements, as well as towards using recycled materials derived from end-of-life tyres.

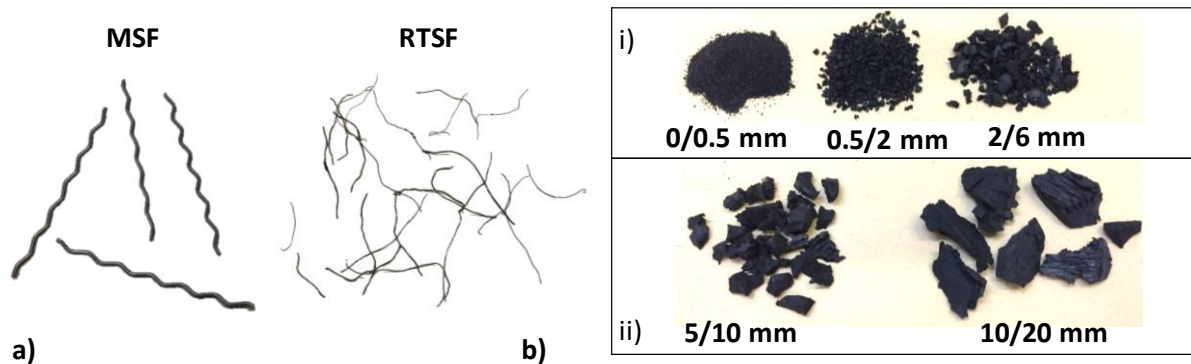
107 **2 Experimental programme**

108

109 **2.1 Materials and casting procedure**

110

111 Four optimised concrete mixes developed previously by the authors [8, 11, 29] were produced  
112 to cast the tested specimens. Three cubes (100 mm) and twelve prisms (100×100×500 mm)  
113 were cast and prepared for each mix. A binder made of 80% of a Portland limestone cement  
114 CEM II-52.5 N, 10% of silica fume (SF) and 10% of pulverised fuel ash (PFA) was used for  
115 all concrete mixes. The fine aggregate was medium-grade washed river sand with size 0/5 mm  
116 and specific gravity (SG) of 2.65, whereas the coarse aggregate was round river washed gravel  
117 with particle sizes of 5/10 mm and 10/20 mm and SG of 2.64. Chemical admixtures including  
118 plasticiser and superplasticiser were utilised to enhance workability and cohesion. A blend of  
119 20 kg/m<sup>3</sup> of MSF (0.8, 55) and 20 kg/m<sup>3</sup> of RTSF (0.22, 23), as shown in Figure 1a, were used  
120 as reinforcement. Details on the characterisations of the steel fibres are reported in [8, 38].

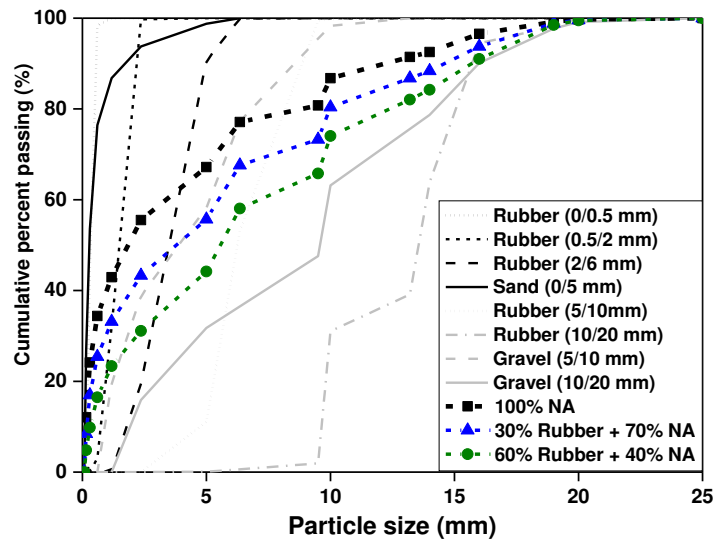


121

122 Figure. 1 a) MSF and RTSF, b) rubber particles, used in this study

123

124 The natural aggregates were replaced with two different volumetric percentages of rubber  
125 particles (30% or 60%) of roughly similar size distribution to minimise packing issues. Figure  
126 1b shows the rubber particles according to size. The fine rubber particles of sizes 0/0.5 mm,  
127 0.5/2 mm and 2/6 mm were used in a 2:3:4 ratio, respectively, whilst the coarse rubber particles  
128 of sizes of 5/10 mm and 10/20 mm were used in a 1:1 ratio. The mass of rubber replacing the  
129 mineral aggregates was calculated using a relative density of 0.8 [8]. Figure 2 shows the particle  
130 size distribution of rubber and natural aggregates (NA) obtained according to ASTM-C136  
131 [39].



132

133 Figure. 2 Particle size distributions for rubber particles and natural aggregates

134 Table 1 summarises the mix proportions and corresponding IDs of the four concrete mixes  
 135 examined in this study. The number in the ID represents the quantity of rubber particles  
 136 replacing both fine and coarse aggregates (0%, 30% or 60% by volume), while P=Plain  
 137 concrete and BF=blend fibres.

138 **Table 1.** Mix proportions for 1 m<sup>3</sup> of concrete, adapted from [8]

Components	Concrete mixes ID			
	<i>OP</i>	<i>0BF</i>	<i>30BF</i>	<i>60BF</i>
CEM II (kg/m <sup>3</sup> )	340	340	340	340
Silica Fume (SF) (kg/m <sup>3</sup> )	42.5	42.5	42.5	42.5
Pulverised Fuel Ash (PFA) (kg/m <sup>3</sup> )	42.5	42.5	42.5	42.5
Fine aggregates 0/5 mm (kg/m <sup>3</sup> )	820	820	574	328
Coarse aggregates 5/10 mm (kg/m <sup>3</sup> )	364	364	254	146
Coarse aggregates 10/20 mm (kg/m <sup>3</sup> )	637	637	446	255
Water (l/m <sup>3</sup> )	150	150	150	150
Plasticiser (l/m <sup>3</sup> )	2.5	2.5	3.25	4.25
Superplasticiser (l/m <sup>3</sup> )	5.1	5.1	5.1	5.1
Fine rubber particles (kg/m <sup>3</sup> )	0	0	165	330
Course rubber particles (kg/m <sup>3</sup> )	0	0	24.8	49.6
MSF (kg/m <sup>3</sup> )	0	20	20	20
RTSF (kg/m <sup>3</sup> )	0	20	20	20
Total	2404	2444	2087	1733

139

140 To produce the SFRRuC mixes, natural and rubber aggregates were first added into a pan mixer  
 141 and mixed for approximately 30 s in dry conditions. Half of the mixing water was then added,  
 142 and the materials were mixed for 1 min. The mixer was halted for three minutes to add the

143 binder materials. Subsequently, mixing restarted and the remaining water and admixtures were  
144 gradually added for another 3 min. Finally, the steel fibres were added manually, and mixing  
145 continued for 3 min. All specimens were cast in moulds using two layers of concrete  
146 (according to EN 12390-2 [40]), and each layer was compacted on a vibrating table for 25 s.  
147 Following casting, the specimens were covered with plastic sheets to retain moisture, and kept  
148 under standard laboratory conditions for 2 days. As a large number of specimens were needed  
149 for each mix, due to parallel durability studies [29, 30], three batches were cast for each mix.  
150 The number of specimens per mix was also limited by the capacity of the concrete mixer in the  
151 laboratory. All specimens were cured in a mist room for 28 days, after which they were stored  
152 under standard laboratory conditions until testing. All specimens were tested after 150 days  
153 following casting to ensure that they had developed their full strength.

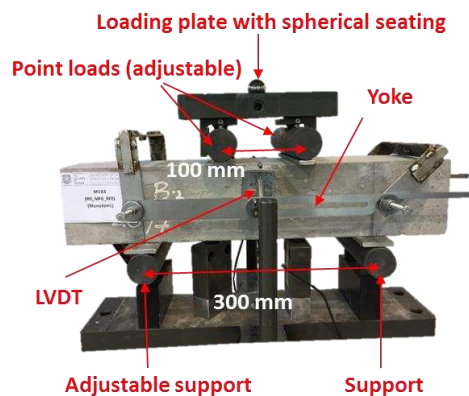
154

## 155 **2.2 Test setup and instrumentation**

156

157 The uniaxial compressive tests on cubes were carried out using a cube crusher at a loading rate  
158 of 0.4 MPa/s, according to EN 12390-3 [41]. The prisms were subjected to static and fatigue  
159 four-point bending using a servo-hydraulic actuator with a capacity of 250 kN ( $\pm 0.05\%$  error).  
160 Two linear variable differential transducers (LVDTs) mounted onto each side of a yoke, as  
161 suggested by the JSCE guidelines [42] (see Figure 3), monitored the vertical mid-span  
162 displacement of the prisms. The static tests were performed at a displacement rate of 0.2  
163 mm/min. Initially, three prisms per mix were tested statically to select the load limits for the  
164 fatigue tests and to monitor the development of cracks. The maximum amplitude of the fatigue  
165 load was calculated by multiplying a stress ratio ( $S=0.5, 0.7$  or  $0.9$ ) by the average flexural  
166 strength obtained from the three specimens subjected to static load. As discussed in more detail  
167 in section 3.3, in some cases the stress ratio was multiplied by the characteristic flexural  
168 strength (instead of the average) to prevent premature failure of the prisms during the fatigue  
169 tests. The minimum amplitude of each loading cycle was set to 10% of the maximum fatigue  
170 load to avoid disengagement of the specimens during testing. The fatigue loading cycles were  
171 applied at a frequency of 15 Hz (sinusoidal wave), which is within the typical range (12-20 Hz)  
172 used for prism tests in order to avoid amplification or resonance problems [1, 19, 36, 43, 44].  
173 The load cycles were applied in four point bending, ensuring a sufficient constant moment  
174 region to allow the development of cracked sections at a known stress level. The fatigue tests  
175 were terminated either after two million cycles, or at failure of the prisms. Readings were saved  
176 at specific logarithmic steps as following (every cycle from 0 to 10 then every 10th cycle up to

177 100 cycles, then every 100th cycle up to 1,000 cycles, then every 1,000th cycle up to 10,000  
178 cycles, then every 10,000<sup>th</sup> cycle up to failure). The main output of the fatigue tests was the  
179 number of cycles at failure as well as the vertical displacements recorded by the LVDTs.



180  
181

Figure. 3 Flexural test set-up

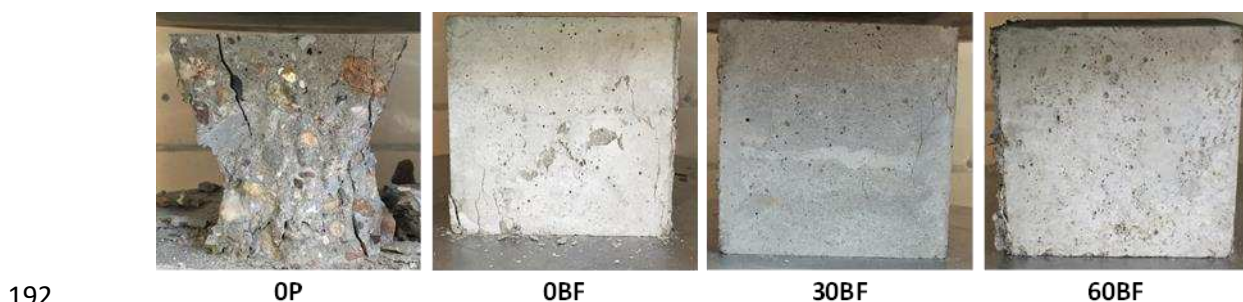
### 182 3 Results and discussion

183

#### 184 3.1 Failure mode

185

186 Typical failure modes of the tested cubes are shown in Figure 4. Whilst the plain concrete  
187 specimens (*OP*) failed in a brittle manner, the SFRC and SFRRuC specimens failed in a much  
188 more ‘ductile’ manner. As the inclusion of large amounts of rubber and steel fibres led to the  
189 development of more distributed (and thinner) cracking, compared to specimens without rubber  
190 (*OP*), this confirms that ductility was improved by adding fibres and further enhanced by the  
191 rubber, as explained previously by the authors in [8].



192  
193

Figure. 4 Typical failure modes of concrete cubes

#### 194 3.2 Static compressive and flexural strengths

195

196 Table 2 summarises the average cube compressive strength ( $f_{cm,cube}$ ), static flexural elastic  
197 modulus ( $E_s$ ), and static flexural strength ( $f_{cm,fl}$ ) including characteristic values ( $f_{ctk,fl}$ ) for each

198 concrete mix. The coefficient of variation is also presented in brackets. The results in Table 2  
 199 indicate that the addition of a blend of steel fibres in conventional concrete (mix *0BF*) increases  
 200 the compressive strength by 18% over the plain concrete mix (*0P*). A similar enhancement was  
 201 observed in a previous study by the authors [8], who attributed the enhancement to the ability  
 202 of steel fibres (especially RTSF) to control and delay micro-crack coalescence and the unstable  
 203 propagation of cracking. However, mixes *0BF* and *0P* show the same elastic modulus and  
 204 flexural strength despite the difference in compressive strength, which may be attributed to  
 205 some air being trapped during the casting of *0BF* prisms as observed by the authors in another  
 206 study [8]. Indeed, the results in [8] showed that the increase in air content creates weaknesses  
 207 inside the concrete matrix and decreases concrete density, which in turn affects both the  
 208 strength and stiffness. Compared to mix *0P*, replacing large amounts of fine and coarse  
 209 aggregates with rubber reduces the compressive strength by 49% and 85% for *30BF* and *60BF*  
 210 mixes, respectively. Similarly, the elastic modulus and flexural strength of mix *30BF* drop by  
 211 57% and 34%, respectively, whereas these properties decrease by 75% and 42% for mix *60BF*.  
 212 Nevertheless, in the design of road pavements, which work essentially in bending, having  
 213 sufficient flexural strength is more important than having high compressive strength, provided  
 214 durability is not compromised.

215 Table 2. Static compressive and flexural test results

Mix	$f_{cm,cube}$ (MPa)	$E_s$ (MPa)	$f_{cm,fl}$ (MPa)	$f_{ctk,fl}$ (MPa)	$\frac{f_{ctm,fl}}{\sqrt{f_{cm,cube}}}$
<i>0P</i>	102 (4.7)	51 (5.1)	7.0 (13.3)	5.2	0.693
<i>0BF</i>	120 (2.9)	51 (4.8)	7.0 (9.3)	5.8	0.639
<i>30BF</i>	52 (7.5)	22 (13.8)	4.6 (5.3)	4.1	0.638
<i>60BF</i>	15 (10.7)	13 (21.9)	4.1 (18.5)	2.6	1.058

216  
 217 The reduction in strength and stiffness in SFRRuC is mainly due to the lower stiffness and  
 218 higher Poisson's ratio of rubber (nearly 0.5) when compared to natural aggregates, but also due  
 219 to the poor adhesion between rubber and cement paste [8, 11, 15]. It should be noted that the  
 220 compressive strength of the mixes degrades faster than the flexural strength, which confirms,  
 221 as also discussed in [8], that the combination of fibres and rubber enhances the tensile capacity  
 222 of SFRRuC. This is evident by noting that the ratio of the average static flexural strength to the  
 223 square root of the average compressive strength ( $\frac{f_{ctm,fl}}{\sqrt{f_{cm,cube}}}$ ) for *60BF* is much higher than for  
 224 the other mixes.

225 It should be mentioned that the relatively large variability in  $f_{cm,fl}$  in Table 2 can be attributed  
 226 to the fact that each specimen belonged to a different batch. To determine a safe initial loading

227 protocol for the fatigue stress loads, the characteristic flexural strength ( $f_{ctk,fl}$ ) of each mix was  
 228 determined according to RILEM TC 162-TDF [45].

229

### 230 3.3 Flexural fatigue strength

231

232 Table 3 summarises the flexural fatigue results of the tested prisms. The results report the stress  
 233 ratio ( $S$ ) in decreasing order, as well as the fatigue life ( $N$ ). For the initial tests (3 prisms per  
 234 mix), the maximum and minimum amplitudes of the fatigue load were determined using the  
 235 characteristic strength values ( $f_{ctk,fl}$ ) and  $S=0.9$  (see footnote \* in Table 3). After examining the  
 236 values  $N$  at this stress ratio, it was found that some of the plain concrete ( $OP$ ) and SFRC  
 237 specimens ( $OBF$ ) sustained at least 2 million cycles. Conversely, the  $N$  values of the SFRRuC  
 238 specimens ( $30BF$  and  $60BF$ ) were much lower. Hence, it was decided to use average strength  
 239 values ( $f_{ctm,fl}$ ) and  $S$  of 0.8 and 0.9 for the tests on prisms  $OP$  and  $OBF$ , respectively. On the  
 240 other hand, the flexural fatigue loads for the tests on prisms  $30BF$  and  $60BF$  were determined  
 241 using characteristic values and  $S$  of 0.7 and 0.5.

242

243

Table 3. Fatigue flexural test results

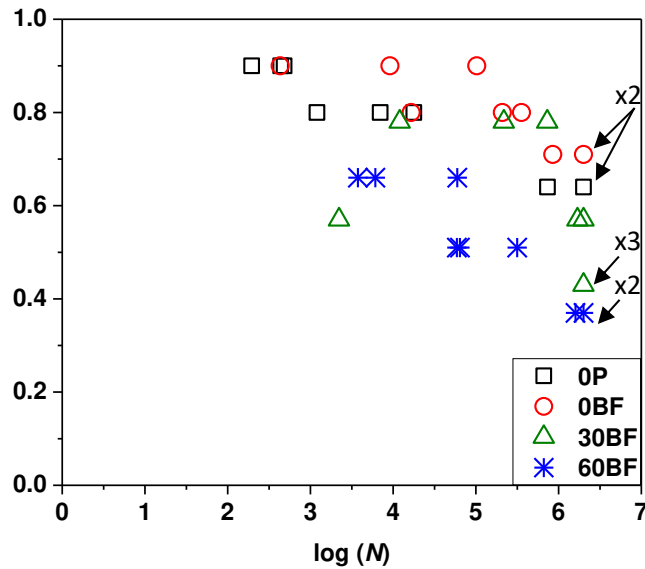
Mix	Stress ratio, $S$ , based on $f_{ctm,fl}$ ( $f_{ctk,fl}$ )	Specimen No.	Fatigue life, $N$	Mix	Stress ratio, $S$ , based on $f_{ctm,fl}$ ( $f_{ctk,fl}$ )	Specimen No.	Fatigue life, $N$	
$OP$	0.9 (1.26)	$OP$ -1	195	$30BF$	0.78 (0.9*)	$30BF$ -1	12,000 <sup>+</sup>	
		$OP$ -2	438			$30BF$ -2	217,700 <sup>+</sup>	
		$OP$ -3	482			$30BF$ -3	729,700 <sup>+</sup>	
	0.8 (1.12)	$OP$ -1	1,200 <sup>+</sup>		$30BF$	0.57 (0.65)	$30BF$ -1	2,218
		$OP$ -2	6,968				$30BF$ -2	1,690,882
		$OP$ -3	17,800 <sup>+</sup>				$30BF$ -3	2,000,000
	0.64 (0.9*)	$OP$ -1	733,303		$30BF$	0.43 (0.5)	$30BF$ -1	2,000,000
		$OP$ -2	2,000,000				$30BF$ -2	2,000,000
		$OP$ -3	2,000,000				$30BF$ -3	2,000,000
$OBF$	0.9 (1.13)	$OBF$ -1	431	$60BF$	0.66 (0.9*)	$60BF$ -1	3,754	
		$OBF$ -2	9,172			$60BF$ -2	6,084	
		$OBF$ -3	102,718			$60BF$ -3	59,690	
	0.8 (1.0)	$OBF$ -1	16,525		$60BF$	0.51(0.7)	$60BF$ -1	58,937
		$OBF$ -2	209,338				$60BF$ -2	64,157
		$OBF$ -3	356,807				$60BF$ -3	315,080
	0.71 (0.9*)	$OBF$ -1	852,009		$60BF$	0.37(0.5)	$60BF$ -1	1,600,000
		$OBF$ -2	2,000,000				$60BF$ -2	2,000,000
		$OBF$ -3	2,000,000				$60BF$ -3	2,000,000

244 <sup>+</sup> Number of cycles recorded in 100 cycle accuracy.

245 \* Initial tests at  $0.9f_{ctk,fl}$

246

247 Figure 5 compares the logarithmic number of cycles ( $\log N$ ) endured by each specimen and the  
 248 relative  $S$  calculated using  $f_{ctm,fl}$  (quantitative comparisons are included in section 4). It is  
 249 evident that the fatigue life data have a large scatter even for the same mixes and stress ratios,  
 250 in particular for specimens with steel fibres and/or rubber particles. Though the uneven  
 251 distribution of rubber and fibre orientation may significantly contribute to this high variability  
 252 [1, 20], the fact that specimens from different batches were used also plays a significant role.



253

254 Figure. 5 Test results in terms of logarithmic number of cycles ( $\log N$ ) and  $S$  (based on  $f_{ctm,fl}$ )

255

256 Figure 5 indicates that steel fibre blends improve the performance of specimens *OBF* by  
 257 increasing its fatigue life. Previous research has proven that RTSF are effective in restraining  
 258 the propagation of micro-cracks into meso-cracks, whilst MSF are more effective in holding  
 259 macro-cracks together [1, 38].

260

261 The replacement of natural aggregates with rubber in SFRRuC significantly degrades the  
 262 fatigue performance of specimens *30BF* and *60BF*. This can be attributed to the stiffness and  
 263 strength degradation in the SFRRuC resulting from the different elastic properties of rubber,  
 264 as well as to the weak bond between cement paste and rubber. SFRRuC is also highly porous  
 265 [29], which also contributes to stiffness degradation during cyclic loading.

266

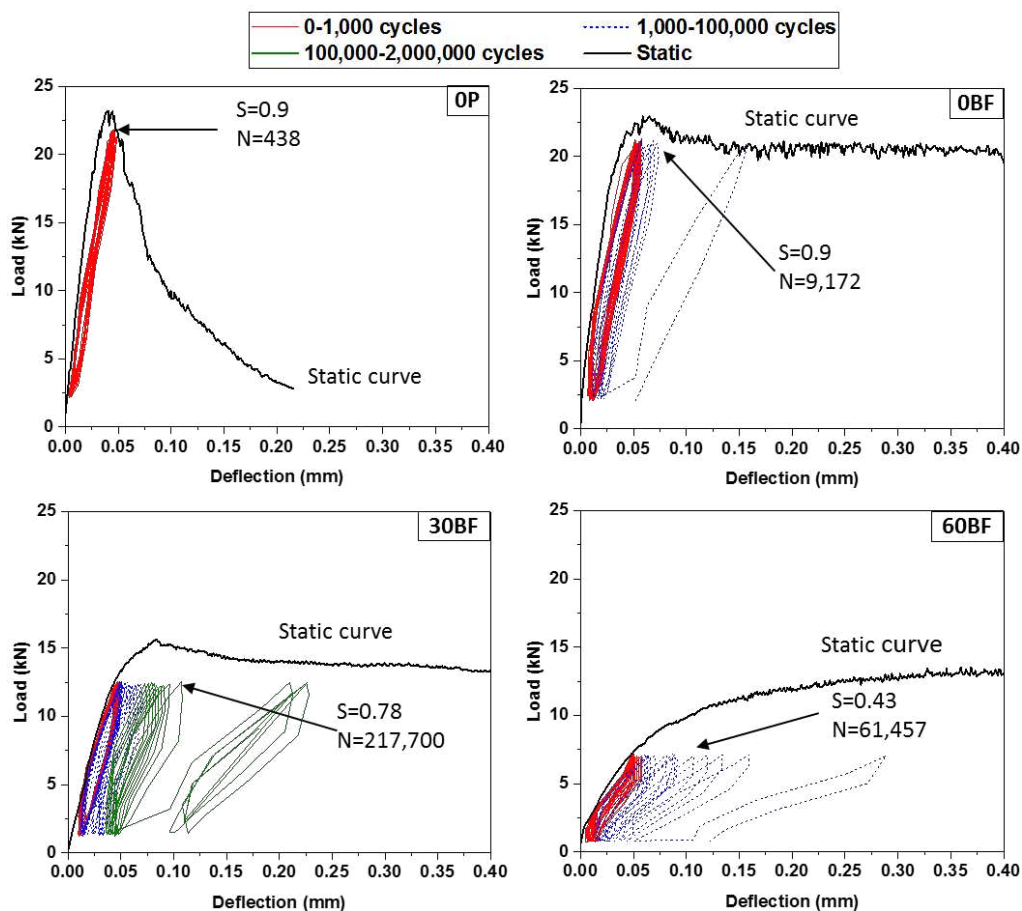
267 Figure 6 compares the load-deflection response under static and fatigue load for the examined  
 268 mixes. The static curve is the average of three prisms, whereas the fatigue curve (one specimen)  
 269 is representative of typical behaviour observed during the tests. Despite the fact that the applied  
 270  $S$  (calculated using  $f_{ctm,fl}$ ) is different for all mixes, it is evident that the initial stiffness (slope)

271 of the fatigue loops is similar to that of the static curve. However, the stiffness degrades  
 272 gradually with the number of fatigue cycles. Note also that the stiffness degrades faster with  
 273 increasing rubber contents. It is also interesting to note that the *OP* and *OBF* failure occurred  
 274 when the fatigue cycles touched the monotonic envelope. This may also be the case for *30BF*  
 275 and *60BF* as one cycle was recorded for every logarithmic step. Though this does not  
 276 necessarily help to predict fatigue life, but it can give an indication of the likely fatigue  
 277 behaviour and, most importantly, the maximum displacement at failure.

278

279 The damage process in SFRRuC under fatigue loading is expected to progress in three stages:  
 280 1) during the first load cycles, flaws and micro-cracks form at the rubber/matrix interface and  
 281 at the weak region within the concrete; 2) as loading progresses, micro-cracks develop at the  
 282 rubber/matrix interface and at the fibre/matrix interface, with the former propagating at a faster  
 283 rate. Although the fibres resist the opening of numerous micro-cracks, these tend to propagate  
 284 and combine quickly to form macro-cracks; 3) at the final stages of loading (or at failure), a  
 285 main crack develops after a sufficient number of macro-cracks have formed.

286



287

288 Figure. 6 Load-deflection response under static and fatigue load for examined mixes

289 The fatigue loops of the SFRRuC (30BF and 60BF) specimens are evidently “fatter” than those  
290 of *OP* and *OBF*, thus indicating that the addition of rubber enhances energy dissipation.  
291 However, a direct comparison of the energy dissipated by the specimens is not possible due to  
292 the different *S* applied during the tests. Note also that, due to their higher flexibility, SFRRuC  
293 specimens exhibit notably higher deflection at failure than that of normal concrete (*OP* and  
294 *OBF*). Despite the lower fatigue resistance of SFRRuC mixes with large volumes of rubber,  
295 their higher ductility and flexibility can still be used to accommodate subgrade movements of  
296 pavement slabs at lower stress levels. To assess the overall fatigue performance of SFRRuC  
297 pavement, a probabilistic approach can be adopted, as shown in the following sections.

298

## 299 **4 Determination of fatigue-life distribution using probabilistic analysis**

300

301 In this section, three models: 1) two-parameter Weibull distribution model, 2) graphical  
302 interpolation model and 3) the mathematical model are used to derive probabilities of failure  
303 ( $P_f$ ) and  $S-N$  relationships for each mix, which can be used in pavement design. For comparison  
304 purposes, the  $P_f-S-N$  relationships are compared at probabilities of failure of 25% and 50% (or  
305 survival probabilities of 75% and 50%, respectively). These values are widely adopted in the  
306 fatigue design of pavements [1, 46-48]. In pavement design, it is usually considered that  $2 \times 10^6$   
307 cycles correspond to an infinite fatigue life [7, 20, 49] and this assumption is utilised in the  
308 following calculations.

309

### 310 **4.1 Two-parameters Weibull distribution**

311

312 The Weibull distribution has been widely used for the statistical analysis of fatigue life data in  
313 concrete [7, 36, 49, 50] because it is easy to apply, it is statistically sound and provides accurate  
314 results even with a small number of samples, and it has a hazard function that reflects the actual  
315 material behaviour in fatigue. The two-parameters of the Weibull distribution ( $\alpha$  and  $u$ ) can be  
316 calculated through either i) the graphical method, ii) the method of moments, or iii) the method  
317 of maximum-likelihood estimate. In this study, the fatigue life data for each mix and at a given  
318 stress ratio  $S$  (based on  $f_{ctm,fl}$ ) are analysed, and  $\alpha$  and  $u$  are estimated using methods i to iii  
319 above. The mean values of  $\alpha$  and  $u$  (average of i to iii) are used to estimate the fatigue lives  
320 corresponding to  $P_f = 0.25$  and  $0.50$ , from which the  $P_f-S-N$  relationships are derived.

### 321 4.1.1 Graphical method

322

323 The Weibull distribution survival function is defined by [7, 50]:

$$324 P_s(N) = \exp \left[ - \left( \frac{N}{u} \right)^\alpha \right] \quad (1)$$

325 where  $N$  is the fatigue life,  $\alpha$  is the shape parameter (or Weibull slope) at the stress ratio  $S$ , and  
326  $u$  is the scaling parameter (or characteristic life) at  $S$ .

327 By taking the logarithm twice on both sides of Eq. (1):

$$328 \ln \left[ \ln \left( \frac{1}{P_s} \right) \right] = \alpha \ln(N) - \alpha \ln(u) \quad (2)$$

329 If it is assumed that  $Y = \ln \left[ \ln \left( \frac{1}{P_s} \right) \right]$ ,  $X = \ln(N)$  and  $\beta = \alpha \ln(u)$ , then Eq. (2) can be  
330 rewritten as a linear equation:

$$331 Y = \alpha X - \beta \quad (3)$$

332 where all the variables are as defined before. Hence, when the fatigue life data at a given stress  
333 follow a linear trend (correlation coefficient  $r \geq 0.9$ ), such data are deemed to comply with the  
334 Weibull distribution and  $\alpha$  and  $u$  can be obtained directly from regression analyses [7, 20].  
335 Table 4 summarises the fatigue life data (in ascending order),  $P_s$ ,  $X$  and  $Y$  of the tested  
336 specimens. In this table, the survival probability  $P_s$  is calculated using [49, 50]:

$$337 P_s = 1 - \frac{i}{K + 1} \quad (4)$$

338 where  $i$  is the failure order number, and  $K$  is the number of specimens tested at a given stress  
339 ratio ( $K=3$  prisms).

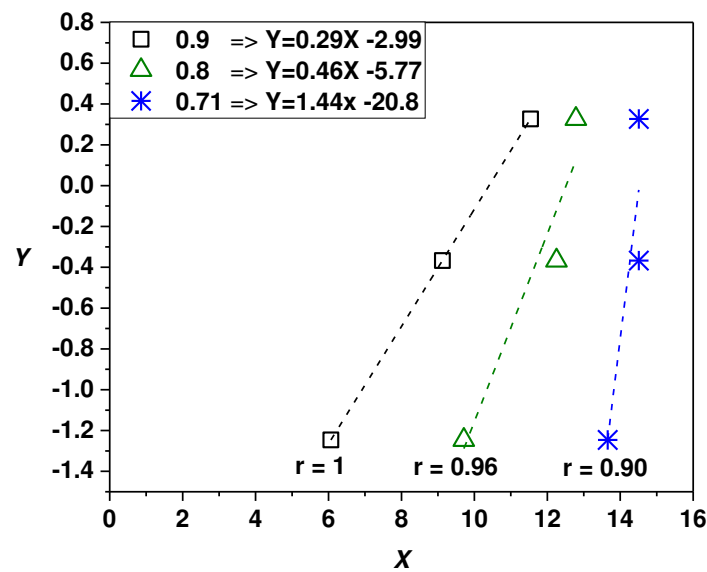
340

Table 4. Analysis of fatigue life data

Mix	S	Fatigue life, N	P <sub>s</sub>	X	Y	Graphical method			Method of moments		Maximum likelihood moment		Average		Estimated fatigue life, N <sub>e</sub> at P <sub>f</sub> of	
						r	α	u	α	u	α	u	α <sub>w</sub>	u <sub>w</sub>	0.25	0.50
OP	0.9	195	0.75	5.27	-1.25	0.94	1.48	461	2.58	419	3.63	415	2.54	427	262	370
		438	0.50	6.08	-0.37											
		482	0.25	6.18	0.33											
	0.8	1,200	0.75	7.09	-1.25	0.99	0.57	11,208	1.03	8,758	1.13	9,029	0.90	9,569	2,400	6,371
		6,968	0.50	8.85	-0.37											
		17,800	0.25	9.79	0.33											
0.64	733,303	0.75	13.51	-1.25	0.90	1.22	2,032,791	2.29	1,780,997	3.18	1,771,850	2.21	1,843,261	1,048,809	1,561,514	
	2,000,000	0.50	14.51	-0.37												
	2,000,000	0.25	14.51	0.33												
OBF	0.9	431	0.75	6.07	-1.25	1.00	0.29	32,926	0.64	26,868	0.53	22,143	0.48	27,039	2,014	12,594
		9,172	0.50	9.12	-0.37											
		102,718	0.25	11.54	0.33											
	0.8	16,525	0.75	9.71	-1.25	0.96	0.46	272,603	1.15	204,081	1.06	198,163	0.88	222,700	54,233	146,979
		209,338	0.50	12.25	-0.37											
		356,807	0.25	12.78	0.33											
0.71	852,009	0.75	13.66	-1.25	0.90	1.44	2,028,617	2.62	1,820,457	3.74	1,804,209	2.57	1,865,583	1,149,396	1,617,843	
	2,000,000	0.50	14.51	-0.37												
	2,000,000	0.25	14.51	0.33												
30BF	0.78	12,000	0.75	9.39	-1.25	0.99	0.37	396,881	0.86	295,090	0.76	278,790	0.66	320,351	47,821	183,078
		217,700	0.50	12.29	-0.37											
		729,700	0.25	13.50	0.33											
	0.57	2,218	0.75	7.70	-1.25	0.91	0.18	1,999,505	1.16	1,295,849	0.47	818,064	0.60	1,357,428	169,741	736,371
		1,690,882	0.50	14.34	-0.37											
		2,000,000	0.25	14.51	0.33											
0.43	2,000,000	0.75	14.51	-1.25	0.00 <sup>+</sup>	0.00 <sup>+</sup>	0.00 <sup>+</sup>	0.00 <sup>+</sup>	0.00 <sup>+</sup>	0.00 <sup>+</sup>	0.00 <sup>+</sup>	0.00 <sup>+</sup>	0.00 <sup>+</sup>	2,000,000	2,000,000	
	2,000,000	0.50	14.51	-0.37												
	2,000,000	0.25	14.51	0.33												
60BF	0.66	3,754	0.75	8.23	-1.25	0.91	0.49	26,817	0.71	18,660	0.84	20,913	0.67	21,909	3,434	12,701
		6,084	0.50	8.71	-0.37											
		59,690	0.25	11.00	0.33											
	0.51	58,937	0.75	10.98	-1.25	0.85 <sup>*</sup>	0.71	193,571	1.00	145,901	1.29	159,403	0.99	164,629	46,870	113,763
		64,157	0.50	11.07	-0.37											
		315,080	0.25	12.66	0.33											
0.37	1,600,000	0.75	14.29	-1.25	0.90	5.49	2,007,453	9.55	1,965,979	14.25	1,946,702	9.67	1,953,644	1,717,428	1,880,968	
	2,000,000	0.50	14.51	-0.37												
	2,000,000	0.25	14.51	0.33												

<sup>+</sup> All of three specimens recorded 2M fatigue cycles, therefore, all point in the curve are aligned. <sup>\*</sup> Correlation coefficient less than 0.9.

343 Figure 7 plots the values  $X$  and  $Y$  for mix  $OBF$ . The results show that the fatigue life data for  
 344 the same stress ratio follow a linear trend. This confirms that  $\alpha$  represents the slope of the curve,  
 345 while  $u$  can be calculated using the curve intercept point. Similar trends were observed for the  
 346 rest of the data, and the results of  $\alpha$  and  $u$  obtained from the graphical method are listed in  
 347 Table 4. It is shown that in most cases  $r \geq 0.9$ , thus indicating that a linear relationship exists  
 348 between  $X$  and  $Y$ . Since all the three prisms  $30BF$  at  $S=0.43$  reached  $2 \times 10^6$  fatigue cycles, the  
 349 three points in the graph are aligned vertically, thus leading to a zero slope (i.e.  $\alpha=0$ ). Although  
 350  $r=0.85$  for  $60BF$  at  $S=0.51$ , the probabilistic analysis is still carried out and the results are  
 351 subsequently adjusted using the average values of the Weibull distribution parameters, as  
 352 explained later.



353  
 354 Figure. 7 Graphical analysis of fatigue-life data for  $OBF$

#### 356 4.1.2 Method of moments

357  
 358 This method calculates  $\alpha$  and  $u$  at each stress ratio using the mean ( $\mu$ ) of three prisms, and the  
 359 corresponding coefficient of variation ( $CV$ ) according to the following equations [36, 49-51]:

$$360 \alpha = (CV)^{-1.08} \quad (5)$$

361 and

$$362 u = \frac{\mu}{\Gamma\left(\frac{1}{\alpha} + 1\right)} \quad (6)$$

363 where  $\Gamma(\cdot)$  is the gamma function.

364 Table 4 summarises the values  $\alpha$  and  $u$  for all concrete mixes at various stress ratios using the  
365 method of moments.

366

### 367 **4.1.3 Method of maximum-likelihood estimate**

368

369 The probability density function of the Weibull distribution can be written as [36, 50, 51]:

$$370 \quad f_N(N) = \frac{\alpha}{\theta} N^{\alpha-1} \exp\left[-\frac{N^\alpha}{\theta}\right] \quad (7)$$

371 where

$$372 \quad \theta = u^\alpha \quad (8)$$

373 The maximum-likelihood function can be expressed as follows [36, 50, 51]:

$$374 \quad \frac{\sum_{i=1}^K N_i^{\alpha^*} \ln(N_i)}{\sum_{i=1}^K N_i^{\alpha^*}} - \frac{1}{\alpha^*} = \frac{1}{K} \sum_{i=1}^K \ln(N_i) \quad (9)$$

$$375 \quad \theta^* = \frac{1}{K} \sum_{i=1}^K N_i^{\alpha^*} \quad (10)$$

376 where  $\alpha^*$  and  $\theta^*$  are the maximum-likelihood estimators for  $\alpha$  and  $\theta$ , respectively, and the rest  
377 of the variables are as defined before. Accordingly, the value  $\alpha^*$  is first obtained iteratively  
378 using Eq. (9), and then replaced in Eq. (10) to calculate  $\theta^*$ . The parameter  $u$  is finally calculated  
379 using  $\alpha^*$  and  $\theta^*$  (instead of  $\alpha$  and  $\theta$ ) in Eq (8). Table 4 summarises the values  $\alpha$  and  $u$  for all  
380 concrete mixes at various stress ratios using the method of maximum-likelihood estimate.

381

382 The results in Table 4 show that the three methods lead to significantly different values of  $\alpha$   
383 and  $u$ , with the graphical method yielding  $\alpha$  and  $u$  values considerably different from those  
384 obtained by the other two methods. This is due to the small number of prisms (three) tested at  
385 each stress ratio, as well as to the large scatter in the fatigue life data. To address this issue and  
386 adopt a more conservative approach, the average values of  $\alpha$  and  $u$  of the three methods are  
387 considered. The average values are shown as  $\alpha_w$  and  $u_w$  in Table 4.

388

389

390 **4.1.4  $P_f$ - $S$ - $N$  relationships**

391

392 The values  $\alpha_w$  and  $u_w$  of the Weibull distribution parameters (Table 4) are used here to estimate  
 393 the fatigue lives corresponding to  $P_f = 0.25$  and  $0.50$  ( $P_s = 0.75$  and  $0.50$ ). The fatigue life  $N_e$  at  
 394 certain  $S$  and  $P_f$  can be estimated using a rearranged version of Eq. (2) [36]:

$$395 \quad N_e = \ln^{-1} \left[ \frac{\ln \left[ \ln \left( \frac{1}{1 - P_f} \right) \right] + \alpha_w \ln(u_w)}{\alpha_w} \right] \quad (11)$$

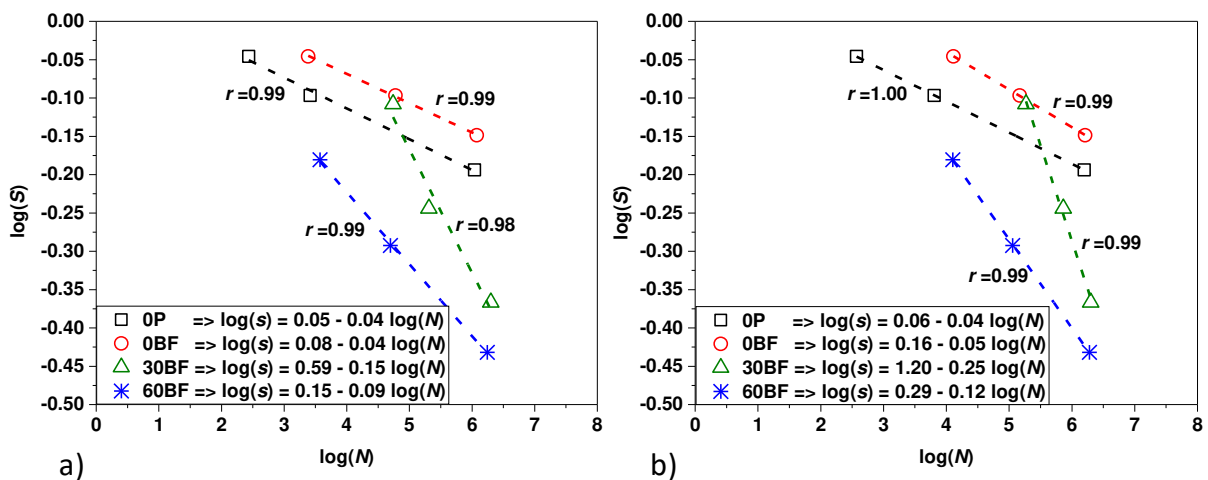
396 Table 4 compares the values  $N_e$  calculated using Eq. (11) at  $P_f = 0.25$  and  $0.50$ . The results  
 397 show that, as expected, for the same stress ratio the value  $N_e$  increases with the probability of  
 398 failure. Additionally, for the same probability of failure,  $N_e$  increases as the stress ratio  
 399 decreases.

400

401 Using the estimated fatigue lives  $N_e$  in Table 4, the  $P_f$ - $S$ - $N$  relationships can be derived using  
 402 the double logarithmic fatigue equation, which has been used in previous studies [7, 19]:

$$403 \quad \log(S) = a + b \log(N_e) \quad (12)$$

404 Figure 8 shows the calculated  $P_f$ - $S$ - $N$  relationships for all concrete mixes using  $N_e$  values at  
 405  $P_f = 0.25$  and  $0.50$ . The constants  $a$  and  $b$  in Eq. (12) are obtained from regression analyses of  
 406 the data shown in Figure 8. It is shown that  $r$  is always close to 1 for all concrete mixes at both  
 407 probability of failures, which confirms the linear trend of the test data. Note that the equations  
 408 in Figure 8 can be used to calculate the stress ratio for a known fatigue life at  $P_f = 0.25$  and  $0.50$ ,  
 409 as shown in section 4.4.



410

411 Figure. 8 Fatigue curves of all concrete mixes corresponding to a)  $P_f = 0.25$  and b)  $P_f = 0.50$

412 **4.2 Graphical interpolations**

413

414 The graphical interpolation model is suitable for practical design because it presents concisely  
 415 the  $P_f$ - $S$ - $N$  relationships, and it is fast and computationally simple. To generate the  $P_f$ - $S$ - $N$   
 416 relationships, the specimens are initially sorted in ascending order of fatigue life [44, 52, 53].

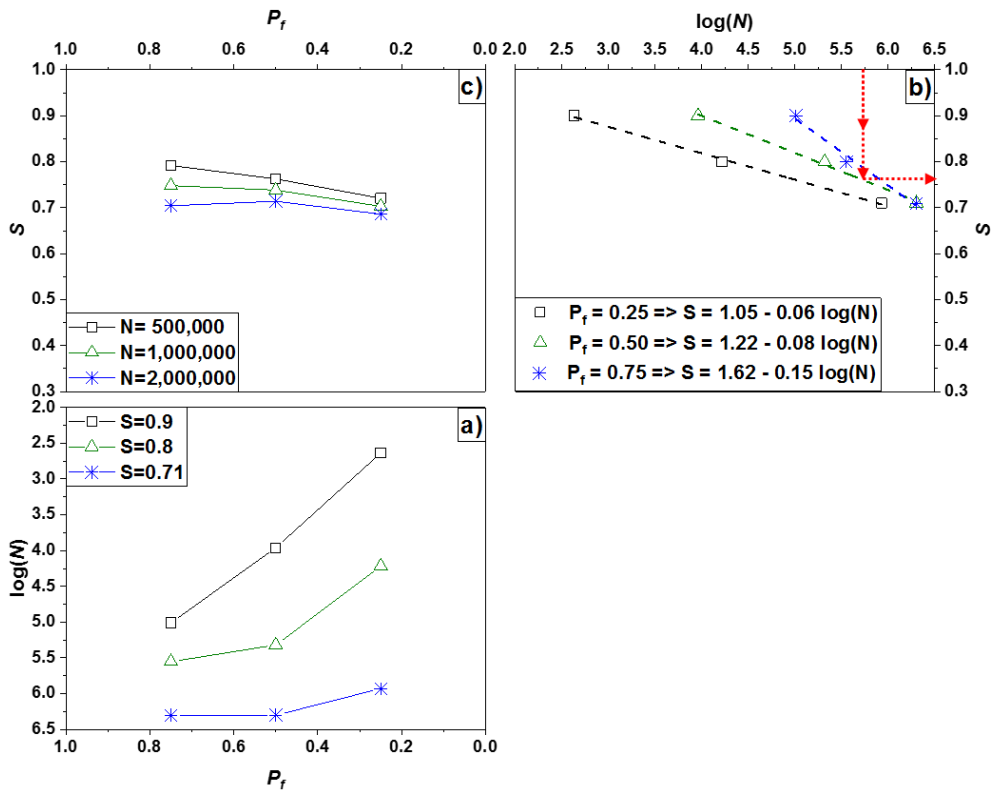
417 The probability of failure is defined as  $\frac{j}{n+1}$ , where  $j$  is the rank of the specimen and  $n$  is the  
 418 number of specimens tested for each mix at a particular stress ratio. Table 5 shows the  
 419 specimens of mix *0BF* ranked according to their fatigue life, as well as the calculated  $P_f$  values.

420 Table 5. Ranked specimens in terms of  $N$  according to stress ratio for mix *0BF*.

$j$	Fatigue life, $N$ , at stress ratio of (based on $f_{cm,t}$ )			$P_f = \frac{j}{(n+1)}$
	0.9	0.8	0.71	
1	431	16,525	852,009	0.25
2	9,172	209,338	2,000,000	0.50
3	102,718	356,807	2,000,000	0.75

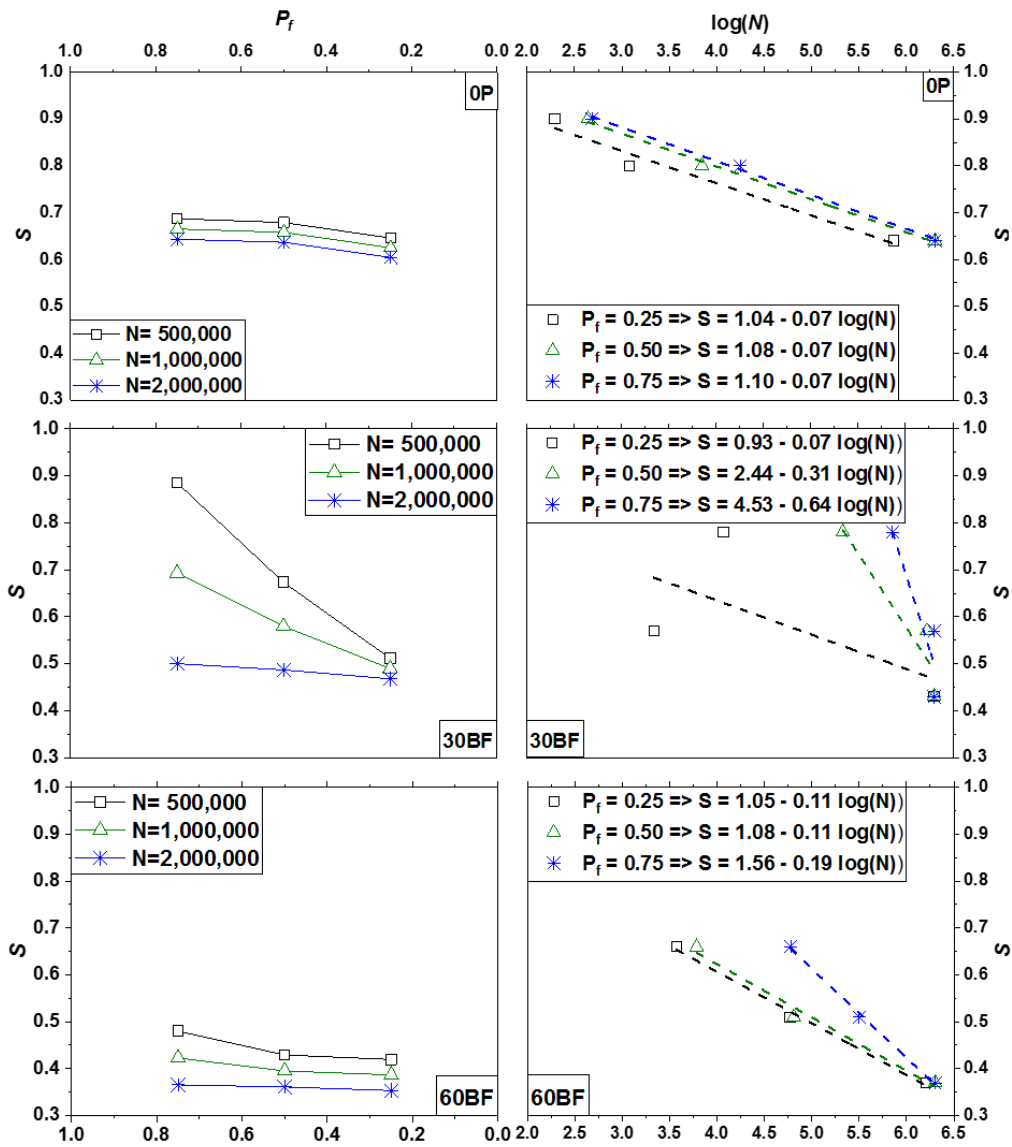
421

422 The  $P_f$ - $S$ - $N$  relationships for mix *0BF* are shown in Figures 9a-c. In this method, a  $P_f$ - $N$  curve  
 423 is initially plotted for each stress ratio using  $P_f$  and  $\log(N)$ , as shown in Figure 9a for the data  
 424 in Table 5. Based on linear regressions, the  $S$ - $N$  curves are then derived using the stress ratios  
 425  $S$  (based on  $f_{cm,t}$ ) and  $\log(N)$  for each  $P_f$ , as shown in Figure 9b. The  $S$ - $P_f$  curves in Figure 9c  
 426 are finally obtained by graphical interpolation for different fatigue lives. For instance, for a  
 427 fatigue life  $N=500,000$  cycles ( $\log(N)=5.7$ ), the estimated stress ratio is  $S_e=0.76$  (see Figure  
 428 9b) for  $P_f=0.50$ . Alternatively, the linear equations obtained by regression analyses in the  $S$ - $N$   
 429 curves (see Figure 9b) can be used to estimate the stress ratio. Different  $N$  can be selected in  
 430 the last step for comparison. In this study,  $N=500,000$ ,  $1,000,000$  and  $2,000,000$  cycles are  
 431 adopted. The  $P_f$ - $S$  and  $S$ - $N$  curves for mixes *0P*, *30BF* and *60BF* calculated following the above  
 432 procedure are shown in Figure 10. Further comparisons of the results shown in Figures 9 and  
 433 10 are included in section 4.4.



434

435 Figure. 9 Graphical interpolation example for mix OBF a)  $P_f$ - $N$ , b)  $N$ - $S$  and c)  $P_f$ - $S$  curves



436

437

438 Figure. 10 Graphical interpolation results for mixes *OP*, *30BF* and *60BF*:  $S$ - $P_f$  and  $S$ - $N$  curves

439

#### 440 4.3 Mathematical models

441

442 Previous research has proposed a mathematical function to derive  $P_f$ - $S$ - $N$  relationships for  
 443 SFRC [1, 44, 52]. The mathematical function can be expressed as:

$$444 P_f = 1 - 10^{-a S^b (\log N)^c} \quad (13)$$

445 where  $a$ ,  $b$  and  $c$  are experimental coefficients derived from statistical analyses of the fatigue  
 446 life data, as described in references [44, 52, 53]. The coefficient  $a$ ,  $b$  and  $c$  obtained for the  
 447 mixes examined in this study are summarised in Table 6. Such coefficients can be replaced in  
 448 Eq. (13) to estimate the stress ratio  $S_e$  for any values of  $N$  and  $P_f$ .

449 Table 6. Experimental coefficients  $a$ ,  $b$  and  $c$  calculated from the mathematical model.

Mix	Experimental coefficients		
	$a$	$b$	$c$
<i>OP</i>	8.77E-04	21.50	8.39
<i>0BF</i>	1.43E-03	10.07	4.76
<i>30BF</i>	2.91E-04	1.71	4.62
<i>60BF</i>	2.27E-06	8.35	10.87

450

451 **4.4 Comparison between models**

452

453 Table 7 compares the estimated fatigue stress ratio  $S_e$  for a fatigue life of  $2 \times 10^6$  cycles and  
 454  $P_f=25\%$  and  $50\%$  obtained from the probabilistic models described in sections 4.1, 4.2 and 4.3.  
 455 With the exception of *30BF*, the estimated fatigue stress ratios obtained from the three models  
 456 agree well for all mixes at the same  $P_f$ . The low stress ratios given by the mathematical model  
 457 for *30BF* can be attributed to the fact that the three specimens for  $S=0.43$  reached  $2 \times 10^6$  fatigue  
 458 cycles (see Table 3), which leads to a very low coefficient  $b$  (see Table 6). The average stress  
 459 ratio of the three models can be used for practical pavement design, as demonstrated by an  
 460 example in the following section.

461 Table 7. Summary of the fatigue stress ratio obtained from three methods.

Mix	$P_f$	Estimated $S_e$ based on			Average stress ratio, $S_{e,ave}$
		Weibull distribution	Graphical interpolation	Mathematical	
<i>OP</i>	25%	0.62	0.60	0.61	0.61
	50%	0.63	0.64	0.64	0.64
<i>0BF</i>	25%	0.70	0.69	0.65	0.68
	50%	0.70	0.71	0.71	0.71
<i>30BF</i>	25%	0.42	0.47	0.24	0.45 <sup>+</sup>
	50%	0.44	0.49	0.40	0.47 <sup>+</sup>
<i>60BF</i>	25%	0.36	0.35	0.34	0.35
	50%	0.37	0.36	0.37	0.37

462 <sup>+</sup> Value calculated based on the Weibull distribution and graphical methods only.

463

464 **5 Design implications**

465

466 To assess the effect of the addition of steel fibres and/or rubber on the thickness  $h$  of rigid  
 467 pavement slabs, a road section with a standard axle load  $W$  is assumed. According to

468 Westergaard's empirical-theoretical model [54], the rigid pavement can be modelled as a thin  
 469 elastic plate on a soil subgrade. The stress at the edge (critical location) is:

$$470 \quad \sigma_{max} = \frac{0.572 W}{h^2} \left[ 4 \log \left( \frac{I}{\sqrt{1.6 Z^2 + h^2} - 0.675 h} \right) + 0.359 \right] \quad (14)$$

471 where  $\sigma_{max}$  is the maximum tensile stress of the slab modified to account for fatigue by  
 472 multiplying the flexural strength ( $f_{ctm,fl}$  listed in Table 2) by the average fatigue stress ratio  
 473  $S_{e,ave}$  at  $P_f=25\%$  (i.e. values from last column in Table 7);  $Z$  is an equivalent contact radius of  
 474 the tyre; and  $I$  is the radius of the relative stiffness of the slab, defined by:

$$475 \quad I = \sqrt[4]{\frac{E_s h^3}{12 (1 - \nu^2) M_k}} \quad (15)$$

476 where  $\nu$  is the Poisson's ratio of the slab material;  $M_k$  is the modulus of elastic subgrade  
 477 reaction; and  $E_s$  is shown in Table 2. In this study,  $M_k$  is the modulus of resilience of the soil  
 478 and measures the ability of the ground to resist immediate elastic deformation under load.

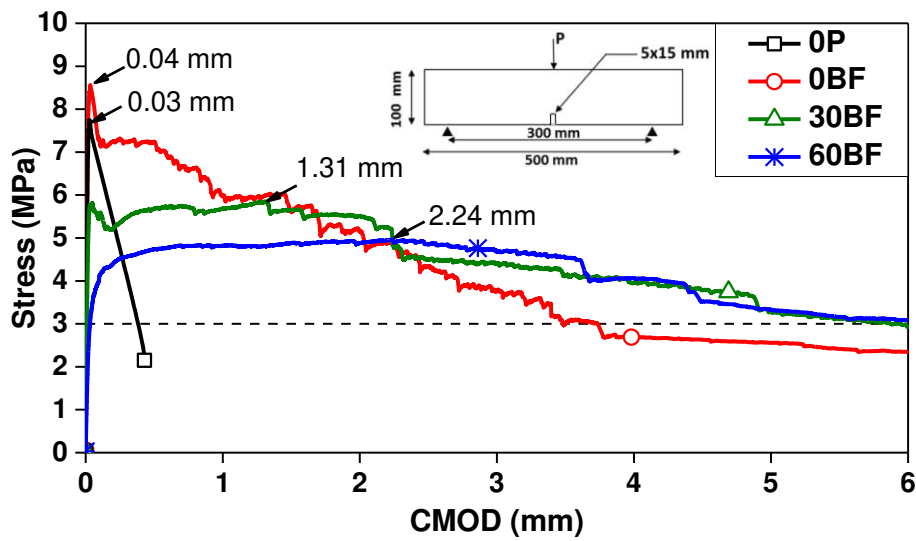
479

480 The slab thickness  $h$  for all concrete mixes was calculated using the modified Westergaard's  
 481 method and the following (typical) values:  $W=80$  kN,  $M_k=80$  MPa/m, and  $Z=190$  mm  
 482 (assuming a tyre pressure of 7 bar), and  $\nu=0.2$ . The subgrade is taken to be a very well  
 483 consolidated made of gravels and sandy gravels [55]. Although mixes *OP* and *OBF* have similar  
 484 average static flexural strength and elastic modulus, the addition of fibres reduces the slab  
 485 thickness by 7% ( $h=173$  mm for *OP* vs  $h=161$  mm for *OBF*). This is mainly due to the enhanced  
 486 fatigue performance resulting from the addition of fibres, as discussed in section 3.3. On the  
 487 other hand, the replacement of natural aggregates with rubber particles increases the slab  
 488 thickness to 256 mm and 305 mm for mixes *30BF* and *60BF*, respectively. This is due to the  
 489 reduced mechanical and fatigue properties of SFRRuC mixes (sections 3.2 and 3.3), which  
 490 leads to a low radius of relative stiffness  $I$  (Eq. (15)).

491

492 Based on these results, it is evident that the modified Westergaard's method does not show the  
 493 expected benefits of using steel fibres and/or rubber over plain concrete. This is because the  
 494 method was originally developed for plain concrete, which behaves in a linear elastic manner  
 495 up to tensile failure. As such, the effect of deformability (i.e. ductility and flexibility) which  
 496 will help to accommodate subgrade movements are not accounted for in the equations. To  
 497 assess the deformability of SFRRuC, the authors performed three-point bending tests on

498 notched prisms according to RILEM [45], and the stress versus crack mouth opening  
 499 displacement (CMOD) curves are shown in Figure 11. The enhancement in flexibility is  
 500 demonstrated by progressively larger CMODs at maximum stress with increasing rubber  
 501 content, resulting from the ability of rubber to reduce stress concentration at the crack tip and  
 502 to delay micro-crack propagation [24]. Likewise, the post-peak behaviour is also improved by  
 503 the inclusion of fibres, and it is further enhanced by the rubber. For example, at a stress level  
 504 of 3MPa, mixes *30BF* and *60BF* have larger CMODs than that of *0BF*, thus confirming the  
 505 enhancement in ductility as discussed in section 3.1. Hence, in order to identify the benefits of  
 506 using steel fibres and/or rubber in concrete, it is necessary to use design equations that take  
 507 into account the flexibility and ductility that SFRRuC can offer.



508  
 509 Figure. 11 Average stress-CMOD curves for prisms

510  
 511 The Technical Report 34 (TR34) by the Concrete Society [56] can be used to show the  
 512 advantages of using SFRRuC pavements. TR34 designs SFRC slabs at the ultimate limit state  
 513 (ULS) using the yield line theory. Accordingly, the flexural moment at the bottom of the slab  
 514 and along the sagging yield lines ( $M_p$ ) are considered to be fully plastic (i.e. residual post-  
 515 cracking behaviour exist), as shown in Eq. (16). At the same time, cracks must be avoided at  
 516 the top surface of the slab and the moment capacity along the hogging yield lines ( $M_n$ ), as  
 517 shown in Eq. (17), should be always greater than the ultimate design moment of the concrete.

518 
$$M_p = \frac{h^2}{1.5} (0.29 \sigma_4 + 0.16 \sigma_1) \quad (16)$$

519 
$$M_n = \frac{f_{ctm,fl}}{1.5} \left( \frac{h^2}{6} \right) \quad (17)$$

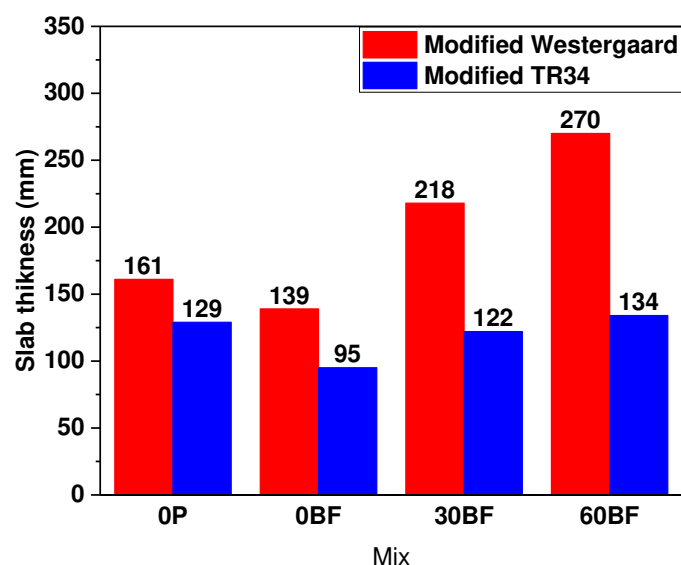
520 where  $\sigma_1 = 0.45 \cdot \text{CMOD}_1$ , and  $\sigma_4 = 0.37 \cdot \text{CMOD}_4$ . In this study, values of  $\text{CMOD}_1 = 0.5$  mm  
 521 and  $\text{CMOD}_4 = 3.5$  mm (as obtained from three-point bending tests on notched prisms [45]) are  
 522 used to calculate  $\sigma_1$  and  $\sigma_4$ . The slab thickness  $h$  can be calculated using Eq. (18) [56] for a  
 523 free edge load.

$$524 \quad W = \frac{[\pi (M_p + M_n) + 4 M_n]}{[1 - (\frac{2Z}{3I})]} \quad (18)$$

525 The design approach adopted by TR34 neglects the effect of fatigue load. To address this  
 526 drawback and account for fatigue, it is thus proposed to modify this approach and multiply  
 527  $f_{cm,fl}$  in Eq. (17) by  $S_{e,ave}$  (section 4.4).

528

529 Figure 12 compares the slab thickness calculated using the modified TR34 approach and  
 530 modified Westergaard's method. It is shown that the adoption of the proposed modified TR34  
 531 approach reduces the slab thickness calculated by the modified Westergaard's method by 20%  
 532 for *OP*, 32% for *0BF*, 44% for *30BF* and 50% *60BF* mixes. These results confirm the benefits  
 533 of using steel fibres and/or rubber in concrete. It is also shown that, although the fatigue  
 534 strength of SFRRuC is relatively low, the thickness of slabs produced with this novel material  
 535 is similar to that of slabs built with plain concrete. However, unlike plain concrete pavements,  
 536 SFRRuC pavements represent a potential solution to accommodate subgrade movements  
 537 during service life. Consequently, it is recommended to use the proposed modified TR34  
 538 approach for the design of flexible SFRRuC pavements.



539

540

Figure. 12 Slab thickness comparison for all concrete mixes

541 The capability of flexible SFRRuC pavements to accommodate subgrade settlements is  
542 demonstrated through finite element (FE) analysis in the following section.

543

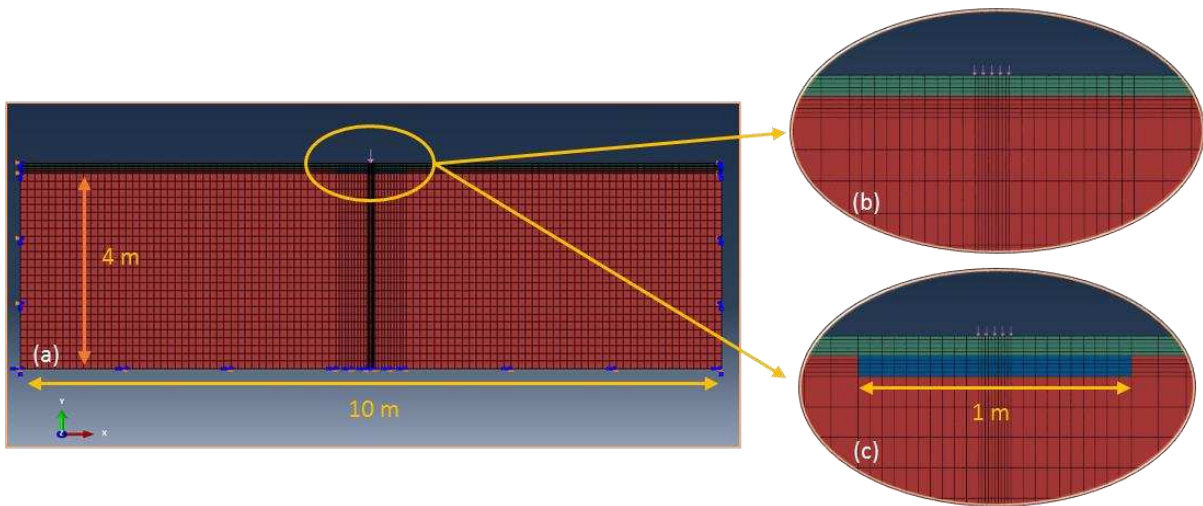
## 544 **6 Finite Element Modelling**

545

546 A two-dimensional (2D) plane strain model of a pavement slab was developed in the FE  
547 software ABAQUS® [57]. Recent research [58] has shown that 2D plane strain models provide  
548 similar results to 3D models (differences of less than 2%) in the study of transverse profiles of  
549 pavements with large longitudinal dimensions. To show the true benefits of flexible SFRRuC,  
550 two pavements designed using the modified TR34 approach (Figure 12) were modelled: i) a  
551 SFRC pavement (*0BF*) of 95 mm depth; ii) a SFRRuC pavement (*60BF*) of 134 mm depth.  
552 The pavements were assumed to be on top of a stiff clay subgrade of length=10.0 m and  
553 depth=4.0 m, as shown in Figure 13a. The length of the pavement was chosen to prevent  
554 boundary and edge effects. Previous research has shown that there are no subgrade  
555 deformations beyond such depth [59]. Two scenarios were considered: 1) a continuous  
556 subgrade (Figure 13b), and 2) a subgrade with a gap filled with loose material (length=1 m,  
557 depth=0.10 m, see Figure 13c). The gap is intended to simulate common defects arising from  
558 non-uniform subgrades due to deterioration developing over time, such as settlement due to  
559 poor compaction during construction or temperature variations and freeze-thaw.

560

561 8-node quadrilateral plane strain reduced integration elements (CPE8R) were used for the  
562 analyses. An initial convergence analysis was performed to optimise the characteristics of the  
563 mesh. Based on these results, only a fine mesh was selected for the loading area. The total  
564 number of nodes and elements was 14962 and 4800, respectively.



565  
 566 Figure. 13 Finite element model: a) discretised pavement and subgrade, b) continuous  
 567 subgrade, c) subgrade with a gap

568

569 The bottom edge of the subgrade was fixed to prevent horizontal and vertical movements. The  
 570 boundary nodes along the pavement edges were constrained horizontally only. A Coulomb  
 571 friction law was used to define the surface-to-surface contact interaction between the pavement  
 572 and subgrade (friction parameter=0.3). The load (standard axle) on the pavement was applied  
 573 through a static contact pressure of 800 kPa. Previous research has widely adopted the Mohr-  
 574 Coulomb plasticity criterion for subgrade analysis [60], hence, this criterion is used to model  
 575 the inelastic behaviour of the subgrade and the filling material in the gap. Table 8 summarises  
 576 the soil properties used in the FE analyses.

577 Table 8. Assumed soil properties used in FE analyses.

Soil	Elastic modulus (MPa)	Poisson's ratio, $\nu$	Friction angle, $\phi$ ( $^{\circ}$ )	Dilation angle $\psi$ ( $^{\circ}$ )	Yield stress (KPa)	Plastic strain
Stiff Clay (subgrade)	80	0.45	0	0	200	0
Loose Sand (hole filling)	10	0.20	28	0	1	0

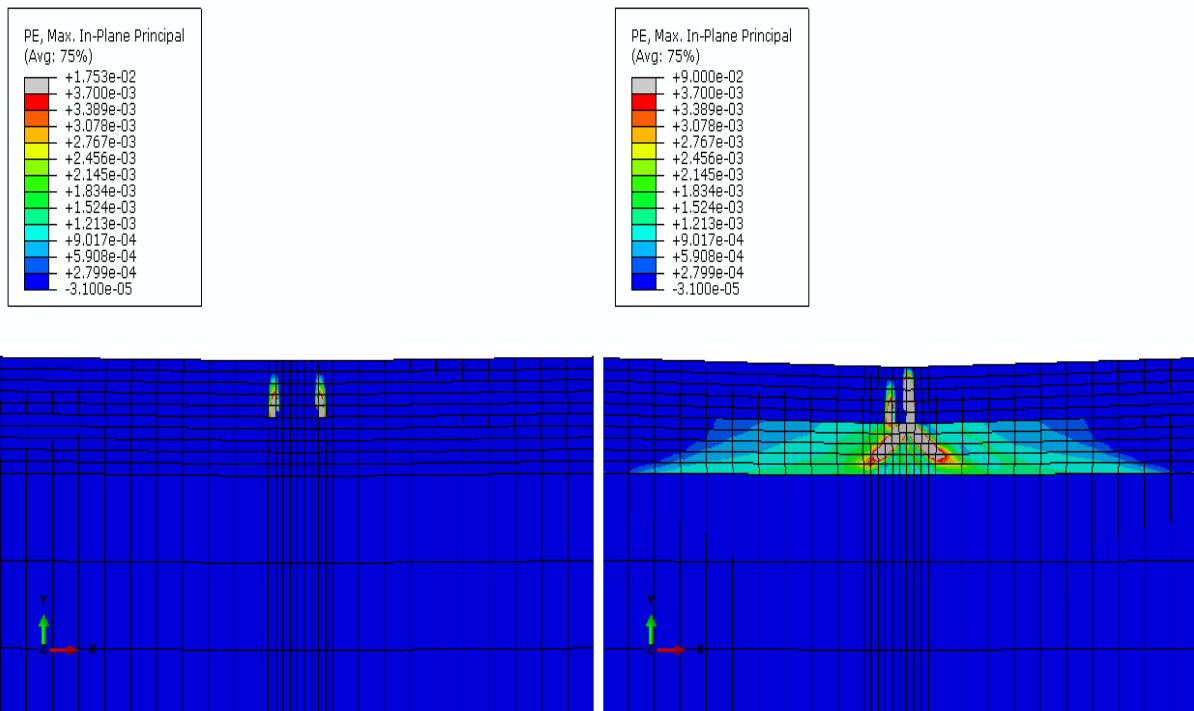
578

579 The concrete was modelled using the concrete damaged plasticity (CDP) constitutive model  
 580 built-in in ABAQUS®. This model accounts for the inelastic behaviour of concrete in both  
 581 tension and compression, and can include damage. The model considers two main failure  
 582 mechanisms in concrete: tensile cracking and compressive crushing. The stress-strain  
 583 relationship for uniaxial concrete in tension was obtained using inverse analysis [61, 62]) on

584 the load-deflection curves presented in Figure 6b and d. The values for the CDP model (dilation  
 585 angle=30, eccentricity=0.1,  $\frac{F_{b0}}{f_{co}} = 1.116$ ,  $K=0.667$  and viscosity= $1 \times 10^{-5}$ ) were taken from  
 586 previous research [61, 63, 64] using SFRC.

587

588 Figure 14 compares the plastic strain distribution (cracks) for the SFRC pavement (*0BF*)  
 589 considering the two scenarios. Whilst wide localised cracks develop in both scenarios, the  
 590 results in Figure 14b indicate that cracks can be up to 5 times wider if a gap develops under the  
 591 pavement. It is also shown that if the pavement settles, two wide cracks propagate through the  
 592 pavement towards its top surface within the loaded area. This implies that the pavement would  
 593 experience significant damage due to multiple wide cracks, thus jeopardising its serviceability  
 594 requirements.

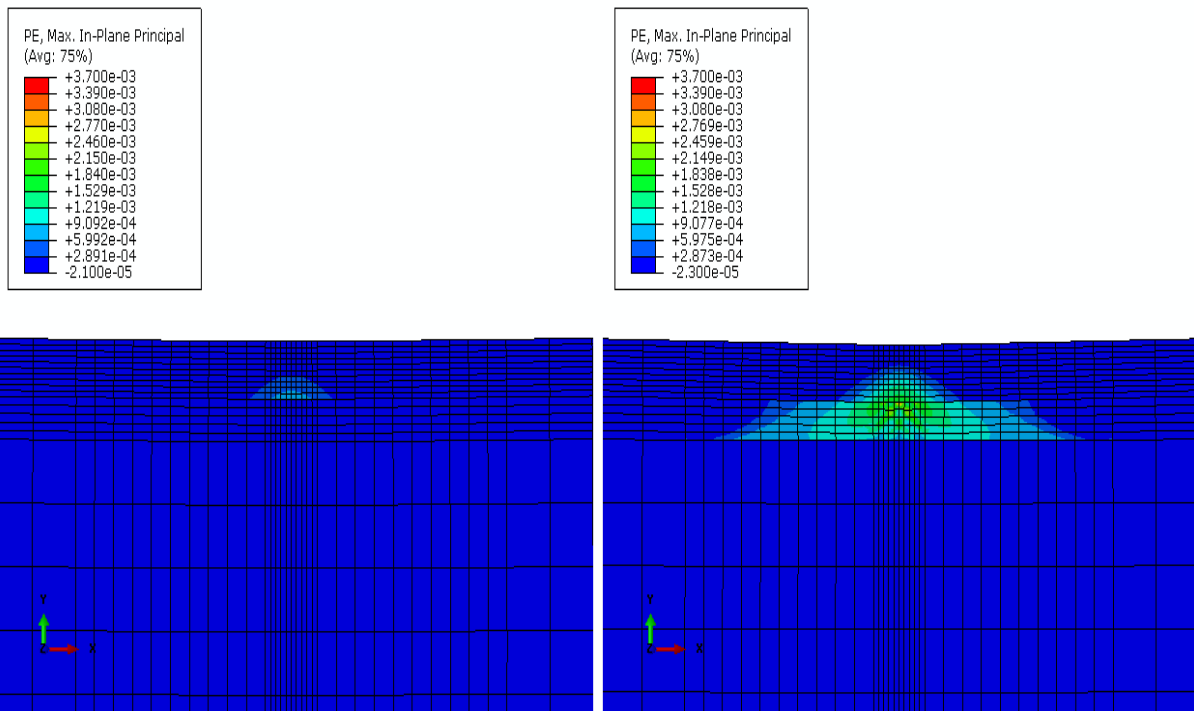


595

596 Figure. 14 Plastic strain model *0BF*-95 mm a) without a gap, and b) with 10 cm × 1 m gap.

597 Figure 15 compares the plastic strain distribution (cracks) for the SFRRuC pavement (*60BF*)  
 598 considering both scenarios. Figure 15a shows that some minor cracks develop in the pavement  
 599 on the continuous subgrade. However, these cracks are more spread and up to 7 times narrower  
 600 compared to the SFRC pavement (see Figure 14a). In presence of the gap (Figure 15b), the  
 601 cracks in the SFRRuC pavement are not only more evenly distributed over a larger area, but  
 602 also significantly narrower (up to 24 times) than those in the SFRC pavement. Even when the  
 603 same depth of 134 mm is used for the SFRC pavement, the cracks are still 10 times larger than

604 the SFRRuC pavement. This shows that flexible SFRRuC pavements are capable of  
 605 accommodating subgrade movements and settlements more effectively than their SFRC  
 606 counterparts.



608 Figure. 15 Plastic strain for model 60BF-134 mm a) without a gap, and b) with 10 cm × 1 m  
 609 gap.

610 It should be mentioned that previous research by the authors showed that optimised flexible  
 611 SFRRuC a) is highly ductile and flexible [8], and b) that such concrete meets the flexural  
 612 strengths specifications defined in pavement design [28]. The authors have also demonstrated  
 613 the adequate durability and long term performance of SFRRuC [29, 30]. In this article, the  
 614 authors prove that (despite its lower fatigue resistance) SFRRuC can accommodate large  
 615 subgrade movements and settlements. The experimental, analytical and numerical evidence  
 616 confirm that SFRRuC is a promising solution for building sustainable road pavements,  
 617 particularly considering that reusing end-of-life tyre materials (WTR and RTSF) in concrete  
 618 can contribute to reducing stockpiles of discarded tyres. It should be also noted that, due to the  
 619 limited number of specimens and mixes examined in the above studies, further research is  
 620 necessary to fully understand the mechanical behaviour and long-term performance of different  
 621 SFRRuC mixes with other mix proportions and tested with different stress ratios (e.g. 6  
 622 specimens tested at each stress level). Current research by the authors is validating the  
 623 predictions given by the modified TR34 approach against additional experiments so as to  
 624 provide practical design guidelines.

## 625 7 Conclusions

626

627 This study assesses the mechanical and fatigue performance of steel fibre reinforced  
628 rubberised concrete (SFRRuC) using fatigue flexural loads on prisms. Based on the results  
629 in this study, the following conclusions are drawn:

630

631 • A blend of steel fibres in concrete enhances its compressive strength by 20%, while the  
632 flexural strength and elastic modulus remain roughly the same. The addition of rubber as  
633 aggregate decreases significantly the compressive strength, static flexural strength and  
634 elastic modulus of SFRRuC. However, the combination of fibres and rubber enhances the  
635 tensile capacity of SFRRuC.

636

637 • The relationships between probability of failure, stress ratio and fatigue life ( $P_f-S-N$ )  
638 given by three probabilistic models widely used in pavement design agree reasonably well.  
639 They also provide comparable estimates of fatigue stress ratios that can be used for the  
640 practical design of SFRRuC pavements.

641

642 • The modified Westergaard's approach does not show the benefits of adding blends of steel  
643 fibres or rubber to concrete since the post-peak behaviour of concrete is neglected. The use  
644 of the modified TR34 design approach proposed in this study leads to thinner slab thickness  
645 when compared to the modified Westergaard's model. Consequently, it is recommended to  
646 use this approach for the design of SFRRuC flexible pavements.

647

648 • FE analyses indicate that flexible SFRRuC pavements can accommodate large subgrade  
649 settlements, thus making such pavements an attractive solution for road pavement  
650 applications.

651

## 652 Acknowledgements

653

654 The authors would also like to thank all of the material suppliers and companies for their in-kind  
655 contribution of materials for this research study: Tarmac UK, Sika, Aggregate Industries UK Ltd,  
656 Twintech, and Twincon Ltd.

657

658 **Disclosure**

659

660 **Funding:** This study was funded by the European Union Seventh Framework Programme  
661 [FP7/2007–2013] under grant agreement no 603722.

662

663

664

665

666

667

668

669

670

671

672

## References

- 675 [1] A.G. Graeff, K. Pilakoutas, K. Neocleous, and M.V.N. Peres, *Fatigue resistance and cracking*  
676 *mechanism of concrete pavements reinforced with recycled steel fibres recovered from post-*  
677 *consumer tyres*, Engineering Structures 45 (2012) 385-395.
- 678 [2] P.C. Perdikaris, A.M. Calomino, and A. Chudnovsky, *Effect of fatigue on fracture toughness of*  
679 *concrete*, Journal of engineering mechanics 112 (8) (1986) 776-791.
- 680 [3] M. Lee and B. Barr, *An overview of the fatigue behaviour of plain and fibre reinforced concrete*,  
681 Cement and Concrete Composites 26 (4) (2004) 299-305.
- 682 [4] O.A. Abaza and Z.S. Hussein, *Flexural Behavior of Steel Fiber-Reinforced Rubberized Concrete*,  
683 Journal Of Materials In Civil Engineering 28 (1) (2015) 04015076.
- 684 [5] T. Nguyen, A. Toumi, and A. Turatsinze, *Mechanical properties of steel fibre reinforced and*  
685 *rubberised cement-based mortars*, Materials & Design 31 (1) (2010) 641-647.
- 686 [6] A. Grinys, H. Sivilevičius, D. Pupeikis, and E. Ivanauskas, *Fracture of concrete containing crumb*  
687 *rubber*, Journal of Civil Engineering and Management 19 (3) (2013) 447-455.
- 688 [7] F. Liu, W. Zheng, L. Li, W. Feng, and G. Ning, *Mechanical and fatigue performance of rubber*  
689 *concrete*, Construction and Building Materials 47 (2013) 711-719.
- 690 [8] A. Alsaif, L. Koutas, S.A. Bernal, M. Guadagnini, and K. Pilakoutas, *Mechanical performance of*  
691 *steel fibre reinforced rubberised concrete for flexible concrete pavements*, Construction and  
692 Building Materials 172 (2018) 533-543.
- 693 [9] S. Raffoul, R. Garcia, D. Escolano-Margarit, M. Guadagnini, I. Hajirasouliha, and K. Pilakoutas,  
694 *Behaviour of unconfined and FRP-confined rubberised concrete in axial compression*,  
695 Construction and Building Materials 147 (2017) 388-397.
- 696 [10] F. Hernández-Olivares, G. Barluenga, M. Bollati, and B. Witoszek, *Static and dynamic*  
697 *behaviour of recycled tyre rubber-filled concrete*, Cement And Concrete Research 32 (10)  
698 (2002) 1587-1596.
- 699 [11] S. Raffoul, R. Garcia, K. Pilakoutas, M. Guadagnini, and N.F. Medina, *Optimisation of*  
700 *rubberised concrete with high rubber content: An experimental investigation*, Construction  
701 and Building Materials 124 (2016) 391-404.
- 702 [12] R. Siddique and T.R. Naik, *Properties of concrete containing scrap-tire rubber—an overview*,  
703 Waste management 24 (6) (2004) 563-569.
- 704 [13] Z. Khatib and F. Bayomy, *Rubberized portland cement concrete*, Journal Of Materials In Civil  
705 Engineering 11 (3) (1999) 206-213.
- 706 [14] A. El-Dieb, M. Abd El-Wahab, and M. Abdel-Hameed, *Mechanical, Fracture, and*  
707 *Microstructural Investigations of Rubber Concrete*, Journal Of Materials In Civil Engineering  
708 (10) (2008) 640-649.
- 709 [15] A.R. Khaloo, M. Dehestani, and P. Rahmatabadi, *Mechanical properties of concrete containing*  
710 *a high volume of tire–rubber particles*, Waste management 28 (12) (2008) 2472-2482.
- 711 [16] E. Ganjian, M. Khorami, and A.A. Maghsoudi, *Scrap-tyre-rubber replacement for aggregate*  
712 *and filler in concrete*, Construction and Building Materials 23 (5) (2009) 1828-1836.
- 713 [17] M.A. Aiello and F. Leuzzi, *Waste tyre rubberized concrete: properties at fresh and hardened*  
714 *state*, Waste Manag 30 (8-9) (2010) 1696-704.
- 715 [18] C. Wang, Y. Zhang, and A. Ma, *Investigation into the fatigue damage process of rubberized*  
716 *concrete and plain concrete by AE analysis*, Journal Of Materials In Civil Engineering 23 (7)  
717 (2010) 953-960.
- 718 [19] F. Liu, L.-y. Meng, G.-F. Ning, and L.-J. Li, *Fatigue performance of rubber-modified recycled*  
719 *aggregate concrete (RRAC) for pavement*, Construction and Building Materials 95 (2015) 207-  
720 217.
- 721 [20] N. Ganesan, J.B. Raj, and A. Shashikala, *Flexural fatigue behavior of self compacting rubberized*  
722 *concrete*, Construction and Building Materials 44 (2013) 7-14.

- 723 [21] F. Hernández-Olivares, G. Barluenga, B. Parga-Landa, M. Bollati, and B. Witoszek, *Fatigue*  
724 *behaviour of recycled tyre rubber-filled concrete and its implications in the design of rigid*  
725 *pavements*, Construction and Building Materials 21 (10) (2007) 1918-1927.
- 726 [22] T. Gupta, A. Tiwari, S. Siddique, R.K. Sharma, and S. Chaudhary, *Response Assessment under*  
727 *Dynamic Loading and Microstructural Investigations of Rubberized Concrete*, Journal Of  
728 Materials In Civil Engineering 29 (8) (2017) 04017062.
- 729 [23] I. Mohammadi, H. Khabbaz, and K. Vessalas, *In-depth assessment of Crumb Rubber Concrete*  
730 *(CRC) prepared by water-soaking treatment method for rigid pavements*, Construction and  
731 Building Materials 71 (2014) 456-471.
- 732 [24] A. Turatsinze, J.L. Granju, and S. Bonnet, *Positive synergy between steel-fibres and rubber*  
733 *aggregates: Effect on the resistance of cement-based mortars to shrinkage cracking*, Cement  
734 And Concrete Research 36 (9) (2006) 1692-1697.
- 735 [25] J.-h. Xie, Y.-c. Guo, L.-s. Liu, and Z.-h. Xie, *Compressive and flexural behaviours of a new steel-*  
736 *fibre-reinforced recycled aggregate concrete with crumb rubber*, Construction and Building  
737 Materials 79 (2015) 263-272.
- 738 [26] N.F. Medina, D.F. Medina, F. Hernández-Olivares, and M. Navacerrada, *Mechanical and*  
739 *thermal properties of concrete incorporating rubber and fibres from tyre recycling*,  
740 Construction and Building Materials 144 (2017) 563-573.
- 741 [27] A. Turatsinze, S. Bonnet, and J.-L. Granju, *Mechanical characterisation of cement-based*  
742 *mortar incorporating rubber aggregates from recycled worn tyres*, Building and environment  
743 40 (2) (2005) 221-226.
- 744 [28] BSI, *EN 13877-1. Concrete pavements Part 1: Materials. BSI 389 Chiswick High Road London*  
745 *W4 4AL UK*, (2013).
- 746 [29] A. Alsaif, S.A. Bernal, M. Guadagnini, and K. Pilakoutas, *Durability of steel fibre reinforced*  
747 *rubberised concrete exposed to chlorides*, Construction and Building Materials 188 (2018) 130-  
748 142.
- 749 [30] A. Alsaif, S.A. Bernal, M. Guadagnini, and K. Pilakoutas, *Freeze-thaw resistance of steel fibre*  
750 *reinforced rubberised concrete*, Construction and Building Materials 195 (2019) 450-458.
- 751 [31] V. Baroghel-Bouny. *Evaluation and prediction of reinforced concrete durability by means of*  
752 *durability indicators. Part I: new performance-based approach. in ConcreteLife'06-*  
753 *International RILEM-JCI Seminar on Concrete Durability and Service Life Planning: Curing,*  
754 *Crack Control, Performance in Harsh Environments. 2006: RILEM Publications SARL.*
- 755 [32] M. Alexander, J. Mackechnie, and Y. Ballim, *Guide to the use of durability indexes for achieving*  
756 *durability in concrete structures*, Research monograph 2 (1999).
- 757 [33] Swedish standards, *SS 13 72 44 ED. 4. Concrete Testing - Hardened Concrete - Scaling At*  
758 *Freezing. Standardiserings-Kommissionen I Sverige*, (2005).
- 759 [34] RILEM, *TC 176-IDC: Internal damage of concrete due to frost action, Final Recommendation,*  
760 *Prepared by L. Tang and P.-E. Petersson SP Swedish National Testing and Research Institute,*  
761 *Boras, Sweden. Materials and Structures / Matériaux et Constructions, Vol. 37, December*  
762 *2004, pp 754-759 in Slab test: Freeze/thaw resistance of concreteInternal deterioration 2004.*
- 763 [35] ETRA, *The European Tyre Recycling Association. 2016, Available at: <http://www.etra-eu.org>*  
764 *[Last accessed: 02/01/2018].*
- 765 [36] S. Goel, S. Singh, and P. Singh, *Fatigue analysis of plain and fiber-reinforced self-consolidating*  
766 *concrete*, Materials Journal 109 (5) (2012) 573-582.
- 767 [37] B.H. Oh, *Fatigue analysis of plain concrete in flexure*, Journal of structural engineering 112 (2)  
768 (1986) 273-288.
- 769 [38] H. Hu, P. Papastergiou, H. Angelakopoulos, M. Guadagnini, and K. Pilakoutas, *Mechanical*  
770 *properties of SFRC using blended manufactured and recycled tyre steel fibres*, Construction  
771 and Building Materials 163 (2018) 376-389.
- 772 [39] ASTM, *C136: Standard test method for sieve analysis of fine and coarse aggregates. ASTM*  
773 *International, West Conshohocken, PA. doi:10.1520/C0136-06. 2006.*
- 774 [40] BSI, *EN 12390-2: Testing hardened concrete, Part 2: Making and curing specimens for strength*  
775 *tests. BSI 389 Chiswick High Road, London W4 4AL, UK. 2009.*

- 776 [41] BSI, *EN 12390-3: Testing hardened concrete, Part3: Compressive strength of test specimens*.  
777 *BSI 389 Chiswick High Road, London W4 4AL, UK*. 2009.
- 778 [42] JSCE, *SF-4: Method of test for flexural strength and flexural toughness of steel fiber reinforced*  
779 *concrete*. Japan Concrete Institute, Tokio, Japan., (1984).
- 780 [43] S. Singh and S. Kaushik, *Flexural fatigue life distributions and failure probability of steel fibrous*  
781 *concrete*, Materials Journal 97 (6) (2000) 658-667.
- 782 [44] S. Singh, B. Ambedkar, Y. Mohammadi, and S. Kaushik, *Flexural fatigue strength prediction of*  
783 *steel fibre reinforced concrete beams*, Electronic Journal of Structural Engineering 8 (1) (2008)  
784 46-54.
- 785 [45] RILEM, *TC 162-TDF: Test and design methods for steel fibre reinforced concrete, Bending test,*  
786 *Final Recommendation. Materials and Structures: 35, 579-582*. 2002.
- 787 [46] B. Zhang, D. Phillips, and K. Wu, *Effects of loading frequency and stress reversal on fatigue life*  
788 *of plain concrete*, Magazine of Concrete Research 48 (177) (1996) 361-375.
- 789 [47] M. Darter and E. Barenberg, *DESIGN OF ZERO MAINTENANCE PLAIN JOINTED CONCRETE*  
790 *PAVEMENT, VOLUME TWO-DESIGN MANUAL*. 1977.
- 791 [48] J.R. Roesler, *Fatigue of concrete beams and slabs*. 1998.
- 792 [49] S. Singh and S. Kaushik, *Fatigue strength of steel fibre reinforced concrete in flexure*, Cement  
793 and Concrete Composites 25 (7) (2003) 779-786.
- 794 [50] B.H. Oh, *Fatigue life distributions of concrete for various stress levels*, Materials Journal 88 (2)  
795 (1991) 122-128.
- 796 [51] Y. Mohammadi and S. Kaushik, *Flexural fatigue-life distributions of plain and fibrous concrete*  
797 *at various stress levels*, Journal Of Materials In Civil Engineering 17 (6) (2005) 650-658.
- 798 [52] S. Singh, B. Singh, and S. Kaushik, *Probability of fatigue failure of steel fibrous concrete*,  
799 Magazine of Concrete Research 57 (2) (2005) 65-72.
- 800 [53] J.T. McCall. *Probability of fatigue failure of plain concrete*. in *Journal Proceedings*. 1958.
- 801 [54] H. Westergaard, *Stresses in concrete pavements computed by theoretical analysis*, Public  
802 roads (1926).
- 803 [55] G. Garber, *Design and construction of concrete floors*. 2006: CRC Press.
- 804 [56] TR34, *The Concrete Society: Concrete industrial ground floors – a guide to design and*  
805 *construction*. 4rd ed. Technical Report 34; 2013.
- 806 [57] Abaqus, *6.14 Abaqus Theory Manual*. USA:Dassault Systemes Simulia Corporation, 651  
807 (2014).
- 808 [58] J. Hua, *Finite element modeling and analysis of accelerated pavement testing devices and*  
809 *rutting phenomenon*, (2000).
- 810 [59] I. ARA, ERES Consultants Division., *Guide for Mechanistic–Empirical Design of New and*  
811 *Rehabilitated Pavement Structures*, Final Rep., NCHRP Project 1-37A (2004).
- 812 [60] H. Jiang and Y. Xie, *A note on the Mohr–Coulomb and Drucker–Prager strength criteria*,  
813 Mechanics Research Communications 38 (4) (2011) 309-314.
- 814 [61] N. Jafarifar, K. Pilakoutas, H. Angelakopoulos, and T. Bennett, *Post-cracking tensile behaviour*  
815 *of steel-fibre-reinforced roller-compacted-concrete for FE modelling and design purposes*,  
816 (2017).
- 817 [62] P. Casanova and P. Rossi, *Analysis and design of steel fiber reinforced concrete beams*,  
818 Structural Journal 94 (5) (1997) 595-602.
- 819 [63] N. Jafarifar, K. Pilakoutas, and T. Bennett, *Moisture transport and drying shrinkage properties*  
820 *of steel–fibre-reinforced-concrete*, Construction and Building Materials 73 (2014) 41-50.
- 821 [64] B. Mobasher, *Mechanics of fiber and textile reinforced cement composites*. 2011: CRC press.
- 822
- 823